Spontaneous Imbibition Processes in Hele-Shaw Cells

José A. Hayashi and Alberto Soria
Dept. de Ingenieria de Procesos e Hidraulica, Universidad Autónoma Metropolitana, Unidad Iztapalapa, Col. Vicentina, CP 09340, México, D.F.

Experiments on spontaneous imbibition processes in Hele-Shaw cells were carried out in squared cells (20 cm × 20 cm) with separations of 0.005, 0.015 and 0.075 cm using twice-distilled water and Soltrol 170 as the displacing and displaced fluids, respectively. The experiments indicated that it was possible to repeat the main features of the spontaneous imbibition process using a procedure for wettability restoration of the glass sheets. The best sweep efficiency was achieved for the 0.015 cm cell gap. Two or three consecutive stages occurred depended on the cell gap, as evidenced by a characteristic speed and a characteristic advancing front structure. The initial stage speed/development stage speed ratio and the oil total area/water-oil total interfacial length ratio as functions of time were gap-dependent. The capillary number and interfacial power density estimations indicated that at about 0.033 cm gap there was a flow pattern transition from slightly uniform displacement to fingering flow.

Introduction

Spontaneous imbibition is defined as the immiscible displacement process by which a wetting fluid displaces a nonwetting fluid that initially saturates a porous or capillary medium, driven only by capillary forces. In the oil industry spontaneous imbibition plays a very important role, particularly in naturally fractured reservoirs and in water-wet rocks. The exchange of water from the fractures and oil towards the fractures is one kind of the matrix-fracture interactions. The more useful modeling expressions are based mainly on global field tests (Aronofsky, 1958; Kazemi et al., 1976) and a lack of the fundamental knowledge of the capillary processes involved is evident. Several authors use the Aronofsky equation in order to simulate the matrix-fracture interaction (de Swaan, 1978; Rodríguez, 1988; Kazemi et al., 1989; Reis and Cil, 1999; Reis and Haq, 1999; Terez and Firoozabadi, 1999). Others benefit from the Kazemi shape factor (Rossen and Shen, 1989; Bech et al., 1991). Others have constructed their own functions (Kleppe and Morse, 1974; Saidi, 1983; Beckner et al., 1987; de Swaan, 1990, 1998).

The experimental research on spontaneous imbibition has been devoted to study this process in reservoir rock samples. Most of the studies have been conducted to obtain information about displacement rates and sweep efficiencies (Brownscombe and Dyes, 1952; Bobek et al., 1958; Mattax and Kyte, 1962; Kleppe and Morse, 1974; Jacquin and Legait, 1984; Cuiec et al., 1990; Zhang et al., 1996). More information has been provided using new techniques for fluid displacement visualization, like gamma-ray absorption (Lefebvre du Prey, 1978), X-ray computerized tomography scanning methods (Bourbiaux and Kalaydjian, 1990; Ramírez, 1998; Akin et al., 2000). Nevertheless, there are still several aspects where research is demanded in order to understand the mechanisms acting in the spontaneous imbibition processes, which determine that a nonwetting fluid may be displaced or left trapped inside the capillary or porous media, especially for the improvement of secondary oil recovery technologies.

Visualization of spontaneous imbibition process is an important tool to study the behavior of the fluid displacement mechanisms inside the capillary or porous media. However, real porous media present many difficulties for *in situ* observation of fluid motion. Taking them as the initial system may be an inconvenient starting point for a basic research study on the governing mechanisms of these processes. Notwithstanding this fact, it is possible that simple models of capillary media may provide relevant basic information that contributes to the understanding of these processes in real porous media (Chatzis and Dullien, 1983; Kalaydjian and Legait, 1988

Correspondence concerning this article should be addressed to A. Soria.
Current address of J. A. Hayashi: Instituto Mexicano del Petróleo, Eje Central Lázaro Cárdenas No. 152, Col. San Bartolo Atepehuacan, 07730, Mexico, D.F.

and Spildo and Buckley, 1999). Furthermore, more information is still needed on spontaneous imbibition in 2-D capillary media (Hayashi and Pérez-Rosales, 1992; Hayashi and Soria, 1995). An approach to remedy this drawback may be by designing *ad hoc* experimental models for the study of the spontaneous displacement characteristics and mechanisms (Hayashi, 2001). For this reason, in this work a 2-D experimental model was built, in order to visualize the spontaneous displacement of oil by water. These simple physical models are known as Hele-Shaw cells and are constructed using two flat parallel transparent sheets with a thin gap between them.

The experimental procedure is described considering (1) the method of wettability restoration; (2) the evaluation of the waviness distribution in Hele-Shaw cells and (3) the experimental development and the fluid properties. Then, (1) studies on the phase motion and the identification of the generated structures by the displacement process are reported; (2) the repeatability of experiments is analyzed through the displacement pattern and the displacement rate; (3) the natural waviness of the system, which might have an influence on fluid displacement, is evaluated; (4) the interface dynamics and its relationship to the displacement speed and the oil-water interfacial length are characterized; and (5) the capillary number and the interfacial power density are found for the characteristic stages of the spontaneous imbibition.

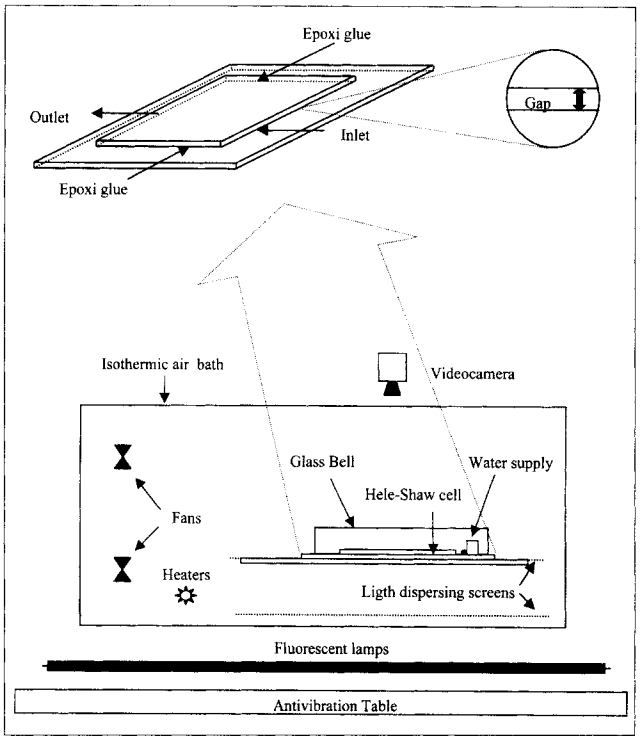

Figure 1. Experimental setup.

Experimental Method

Hele-Shaw cell

The repeatability of the main features of spontaneous imbibition in Hele-Shaw cells needs care on (1) the assembling procedure; (2) the techniques to determine the microstructure gap due to the glass sheets internal surface waviness and (3) the cleanliness and restitution of chemical properties.

Construction. The Hele-Shaw cell consisted of two transparent flat parallel glass plates, with a small gap between them (Figure 1). The Hele-Shaw cell was built with 0.9 cm thick glass sheets and dimensions of 20 cm × 20 cm for the upper sheet and of 30 cm × 40 cm for the lower sheet. Both glass sheets were used for the whole set of experiments, assembling the cell for two G = 0.015 (G being the gap in cm) experiments at first, then for two G = 0.075 experiments, and, finally, for two G = 0.005 experiments, consecutively. The gap between glass sheets was set using nylon thread of several diameters. The upper glass was fixed to the lower one using epoxy glue on two of the upper glass opposite edges and assembling in the identical position as in previous experiments. The cells built in this manner had an inlet and an outlet on opposite sides of a square, as may be appreciated in Figure 1, where the 2-D capillary system is formed by the space between the glass sheets.

Interference Pattern. The glass sheets were used as received from the factory. The only treatment performed was that of cleaning, as described below. However, an optical method was used to obtain information on the magnitude and distribution of the irregularities in the internal surfaces of the cells (waviness). A Fizeau's interferometer, typically used to verify the lens and mirror curvatures, was used for this purpose. Upon placing one glass sheet onto another, as occurs in a Hele-Shaw cell, it is possible to observe the interference map drawn by the gap differences between the internal surfaces. This pattern is a measure of the upper sheet irregularities with respect to the lower sheet irregularities. Thus, the surface waviness of the glass sheets is superposed to a basic gap value, set by a nylon thread with a known diameter. Interference patterns were obtained for G = 0.015 and G = 0.005. It was not possible to define an interference pattern for G = 0.075 due to the apparatus resolution.

Glass Surface Cleaning and Restoration of Chemical Properties. The glass sheets cleaning was one of the most sensitive aspects of this work since it is directly related to the internal surface wettability of the cells. In thermostatics, wettability is defined by the static contact angle between two immiscible phases with a solid surface. However, this concept may be notoriously different for a displacement process (Dussan et al., 1991) since the contact angle should become a dynamic concept, with a dynamic contact line where interfacial tension forces, as well as a line tension force, are balanced. The spontaneous displacement generates complex interfaces that cannot be reproduced in further experiments. Similarity depends on the fact that the capillary structure and the wettability could be accurately restored in order to obtain repeatable conditions at a global level for further experiments. For this reason, the recovery of the geometric and chemical characteristics of the surface was attempted by reconstruction of the 2-D capillary space. This was accomplished by setting the same glass sheets at the same position each time that the cell was assembled and developing a rigorous cleaning procedure to recover the chemical characteristics of the surfaces. This procedure was partially taken from experiences reported by Dussan et al. (1991) for the cleaning of Pyrex glass pipes. First, the glass sheets were submerged for 12 h in a Thinner

solvent bath in order to eliminate fats and oil remains, then the glass sheets were introduced into a diluted Extran M 01 Alkaline (Merck) bath at 20%w, with twice-distilled water to 60°C, for 12 h. Thereinafter, the sheets were rinsed and sponged over with twice-distilled water, after which they were submerged in chromic acid for 12 h, at a concentration of 100 mL of water and 900 mL of sulfuric acid by each 100 g of potassium dichromate. The glass sheets were then rinsed with twice-distilled water and introduced into 50% hydrochloric acid in water for 12 h. In order to restore the surface pH, the sheets were then submerged in a 20% Extran bath at room temperature for 12 h and rinsed and submerged in twice-distilled water for another 12 h after which the glass sheets were again rinsed, rubbed with a wet sponge, and finally dried with nitrogen gas. This procedure had the objective to standardized the chemical properties of the glass sheets.

Experimental Studies

Fluids and their properties

Twice-distilled water was used as the displacing fluid and Phillips Petroleum Soltrol 170 as the displaced fluid. Due to the fact that the Soltrol-water interface is difficult to distinguish at simple sight, an oil soluble pigment was used (Oil Red O BDA from Merck) to emphasize the phase difference, in a concentration of 0.2 g/L. The pigmented oil was filtered with a 0.2 μm pore size micropore filter. The relevant fluid properties such as density, viscosity and interfacial tension, were measured at the temperature of the experiments (25°C). The water viscosity was $\mu = 1.00 \pm 0.005$ cp and the colored Soltrol viscosity was $\mu = 3.80 \pm 0.005$ cp. The interfacial tension between twice-distilled water and colored Soltrol, measured with a Kruss tensiometer, K10 model, was $\sigma = 25.85 \pm 0.005$ dyne/cm. The densities were $\rho = 1.0002 \pm 0.00005$ g/cm^3 for the water and $\rho = 0.7735 \pm 0.00005$ g/cm^3 for the colored Soltrol.

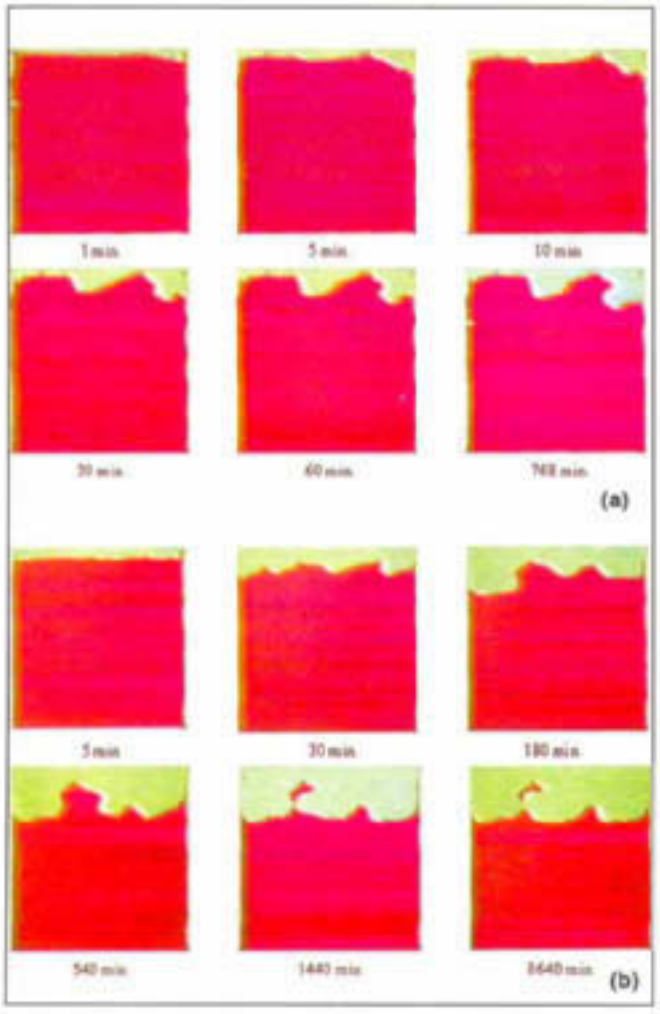

Figure 2. Captured images from Experiments C (a) and D (b) (G = 0.075).

Experimental setup and development

A constant temperature air bath was built to conduct the experiments at controlled temperature, 25 ± 0.5°C. The cell was covered with a glass bell to prevent the disturbances from the circulating air and to reduce the evaporation of liquids, but it was not closed hermetically. Therefore, the experiments were conducted at atmospheric pressure. A Panasonic M9000 video-camera with Super-VHS format was fixed above the cell. The cell lighting was made up by fluorescent lamps set below the cell, and two paper screens were used to generate a dispersed and uniform lighting (Figure 1). A set of representative images from each experiment was selected, captured, and digitally processed with help of a Matrox card and Visiolab 2000 software from Biocom. The experimental setup is shown in Figure 1. Before the experiment started, the capillary space was saturated with colored Soltrol; then, the cell was set horizontally in order to neglect gravity effects and the glass bell was coupled. The experiment started when water was dispensed continuously from the water supply. As the water was flowing into the cell, the water supply provided the required amount of water, in order to maintain the whole inlet in contact with a water film at atmospheric pressure. Since the beginning of the experiment, the whole outlet was in contact with an oil film which was extending on the lower glass sheet, as the Soltrol was being expelled. This oil film was also at atmospheric pressure. As the imbibition process continued, water gradually invaded the capillary space displacing the Soltrol towards the cell outlet.

A first experiment was needed in order to set the initial conditions of the glass surface wettability distribution within the cell. The experiments with a separation of G = 0.075, identified with the letters C and D, are shown in Figure 2. They were performed after two experiments with G = 0.015, identified with the letters A and B, whose sequential advance is shown in Figure 3. The experiments with a separation of G = 0.005 and identified by letters E and F were finally carried out and their sequential advance is shown in the Figure 4. The total time for each experiment is the time interval from the initial water contact with the inlet edge to the final time, when no further configuration changes were observed.

Analysis and Results

Waviness evaluation

The interference pattern, obtained from a Fizeau's interferometer, is a map of the Hele-Shaw cell with iso-lines of

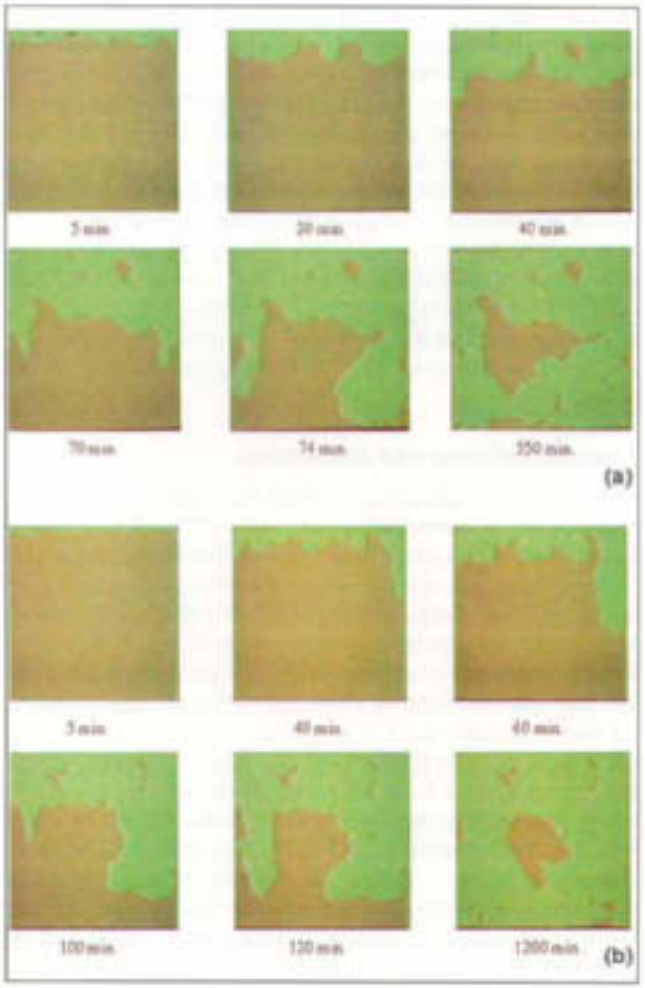

Figure 3. Captured images from Experiments A (a) and B (b) (G = 0.015).

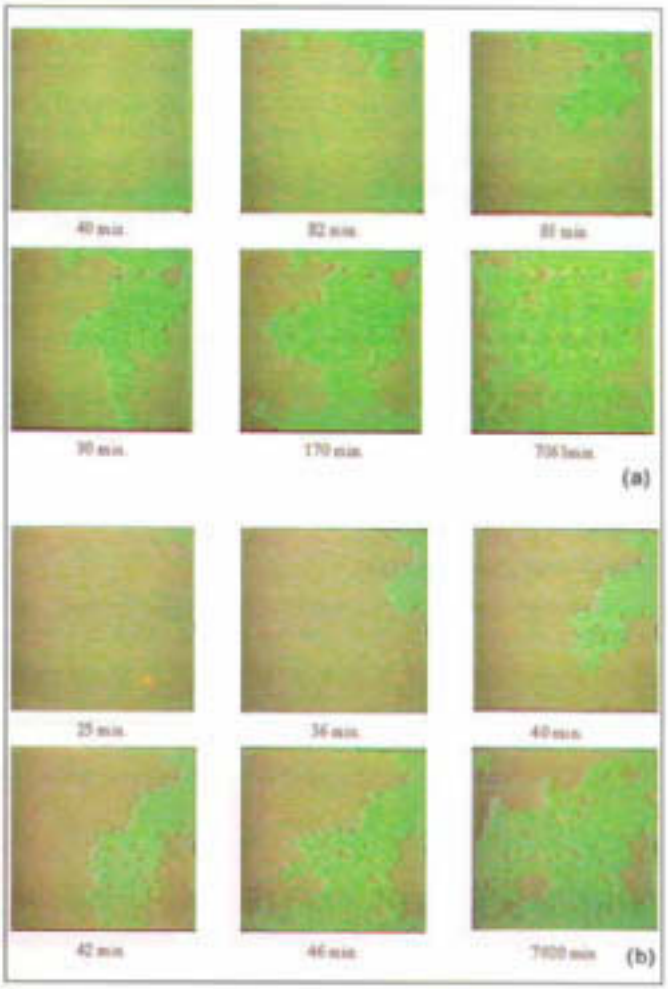

Figure 4. Captured images from Experiments E (a) and F (b) (G = 0.005).

constant-gap that will be referred to as level lines. The number of lines in each cell is presented in Table 1 for each experiment. The waviness magnitude was estimated by the number of level lines in the interference pattern. Between each line couple, there is a distance of $\lambda/2$, λ being the wavelength of the light source ($\lambda \approx 0.5$ μm). The extreme waviness magnitude variations were then estimated, as shown in Table 1, as well as their percentage with respect to the glass sheet gap. In Cell F the greatest percentage in this variation 4.2% was obtained. The capillary pressure changes due to waviness, with respect to the capillary pressure due to the gap was approximately estimated by considering that the capillary pressure is proportional to σ/G, and σ the interfacial tension is assumed to be a constant. Therefore, the capillary pressure changes were estimated from $(1/d_1 - 1/d_2)/(1/G)$, where d_1 and d_2 were the extreme gap values and G was the nominal gap set by the nylon diameter. In this estimation the contact angle was taken as a constant. Considering that the extreme gap variations were much smaller than the nominal gap distance, it may be noted that the capillary pressure changes were in the same magnitude order as the extreme waviness magnitude variations. The importance of waviness for the fluid displacement in the cell was also assessed by direct observation of the imbibition development in the cell, whose interference pattern was known. There did not seem to be a correlation between the level position and the evolution of the interface front. Sometimes, the front advancement was in the orthogonal direction to the level lines and sometimes the advancement was in the tangential direction to these level lines or in any other direction. Moreover, the formation of islands or fingering and their evolution could not have been correlated with the interference map objects such as holes, mounts, valleys, or saddles. Therefore, it was assumed that the glass sheet waviness is not a determining factor for the

Table 1. Interference Pattern Information

Cell	A	B	C	D	E	F
Glass sheet gap, μm	150	150	750	750	50	50
Lines number in cell	66	72	—	—	72	34
Extreme line difference, μm	1.7	1.8	—	—	2.1	0.9
Extreme line difference of cell gap, %*	1.1	1.2	—	—	4.2	1.7

*Also estimated capillary pressure changes due to waviness, with respect to capillary pressure for an imposed cell gap, %.

spontaneous imbibition process reported here. A significant change in the displacement pattern was generated only by a significant change in the glass sheet gap.

Fluid motion and configuration structures

The water-oil interfacial motion generated an advancing front that initially ran throughout the inlet and evolved in time, sometimes leaving in its way fragments of residual oil that remained trapped as islands. These islands could stay fixed, be distorted, coalesce, migrate, or even shrink and disappear, depending on the local wetting conditions and on their sizes, shapes and positions within the cell.

Even though the Hele-Shaw cells are 3-D experimental models, the information obtained from the sequential images of the spontaneous oil displacement by water is 2-D. It was possible to determine perimeter and area for the islands, while for the advancing front, it was better to measure its interface length and the area occupied by oil. The perimeter and the interface length are the *loci* of the water-oil interface and give information about the magnitude and evolution of capillary forces. The time evolution of water and oil areas gives information to quantify the bulk transportation dynamics in the cell, such as the oil expulsion rate (or water-flooding rate) in the cell and the evaluation of the residual oil trapped in the cell at the end of the experiment. The area and the perimeter of the islands left by the advancing front were quantified, as well as the area occupied by oil and the interfacial length at the advancing front in each one of the images. It was assumed that an oil island was formed when the oil phase is fragmented by the surrounding water, leaving it isolated from the rest of the oily phase which continued advancing until it was expelled at the outlet.

At the beginning of the $G = 0.005$ and $G = 0.015$ experiments, it could be observed that the water-oil interface was slightly uniform and advanced slowly. However, once this stage was surpassed, the displacement speed was greater and the advancement was through fingering, as occurred in Experiments A, B, E and F (Figures 3 and 4). In cells with the smallest gap $G = 0.005$, the fingering advance was the fastest and could even increase the fragmentation of the oily phase, with formation of islands, as in Experiments E and F (Figure 4). A different condition was also observed, when the fingering stage did not occur as in Experiments C and D (Figure 2). In this case, after an initial front advancement, the front speed became even slower and finally completely stopped. Under this condition local capillary forces were not able to overcome the viscous resistance.

Two main kinds of oily structures could be identified: (a) a *continuous region*, defined as the oily phase with connection to the cell outlet and (b) an *insular region*, constituted by the fragments of the oily phase left behind as the continuous region advanced toward the outlet. The continuous region was considered to have been disappeared once the outlet had been saturated totally with water, regardless of large islands that may be present inside the cell. This region may be fragmented at the outlet, but each one of the fragments must be in touch with the cell outlet; otherwise, those fragments become part of the insular region.

In the insular region, islands do not have connection with the cell outlet. It was observed that some fragments close to the inlet, to the outlet, or to a closed edge could be distorted and adhered to these sites, re-shaping themselves or even allowing oil to flow outside the cell. For those reasons, the insular region could be characterized as *dynamic or stationary*, according to its evolution. The *dynamic insular sub-region* is the set of islands whose area and perimeter are modified with time. This change may be important since a fragment, considered isolated at a given time, can eventually experience changes in its oil content. This particular situation was observed to occur when the water pushed the fragments that were formed near the inlet, to the outlet or to the closed edges of the cell, helping the fragment to flow outside the cell. The *stationary insular sub-region* is the set of islands whose area is not modified as time elapses. The oil contained in these islands does not vary since the islands are not close to the inlet or the outlet or because a closed edge does not allow oil expulsion. The perimeter of the fragment may be changed with time, but not its area, only a re-shaping of fragments is produced. Two behaviors of these fragments could be observed in the stationary insular sub-region: (a) *static fragments*, whose shape and placement do not change, and whose perimeter and area remain without change. For (b) *migrant fragments* that are mobilized from one site to another within the cell, without oil expulsion, their perimeter, but not their area, changes. Some migrant fragments may eventually be split or coalesced within the cell, re-shaping the stationary sub-region.

Repeatability features analysis

Experiments with $G = 0.005$ (E and F). In Experiments E and F a similar displacement pattern was observed. On the cell righthand side, a quickly growing and advancing finger was developed, crossing the cell in a few minutes (~ 10) and leaving behind a cloud of small scattered oil islands (Figure 4). The final maps of Experiments E are shown in the last slide of each one. There are many islands whose similarities in size and position are apparent. Both experiments were recorded for almost 4 days (7,061 min for Experiment E, and 7,020 min for Experiment F). It was also observed, that when the outlet was water-flooded in both experiments, the oily phase flowed countercurrently towards the inlet, placing a large oil fragment in contact with the inlet edge of the cell. This event may be understood as a large size entrance effect and observations with larger cells should improve or reject this hypothesis.

In Figure 5 the total oil phase area is presented as function of time. Although Experiment E is delayed with respect to Experiment F, the oil expulsion rate is almost the same since the slope of both curves is very close. A change in the slope from this sudden and fast continuous advancement to a slow one may be also appreciated. The former slope is closely related to a notorious decrease in the oil expulsion rate enhanced by countercurrent oil flow towards the cell inlet. Thus, at the end of the experiment, the insular region contributes with a large amount of residual oil. The oil trapped percent was 29.6% for Experiment E and 35.5% for Experiment F.

Experiments with $G = 0.015$ (A and B). The Experiments A and B were recorded in less than one day (550 and 1,200 min, respectively). The final map and the evolution patterns of the experiments were also compared (Figure 3). A great

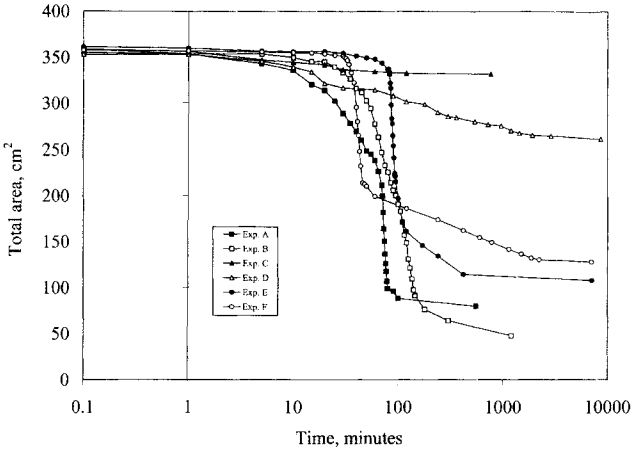

Figure 5. Total oil area for all experiments.

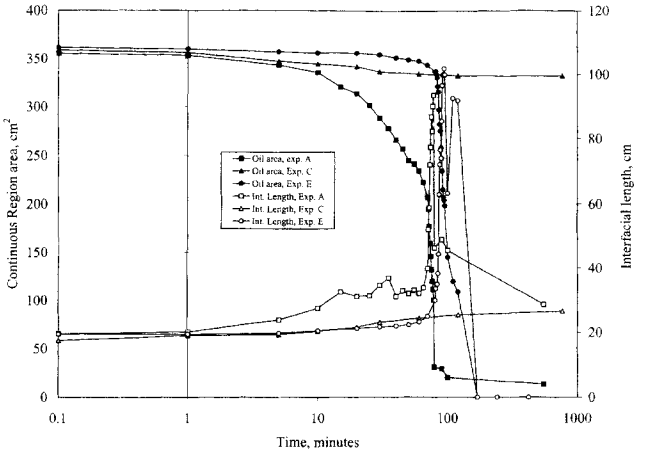

Figure 6. Continuous region area and interfacial length for Experiments A, C and E.

island was apparent in the cell center at the end of the experiments. A fast advancing finger was observed on the right-hand side of the cell in both experiments, which were joined later on another finger that advanced on the lefthand side of the cell.

The behavior of the total oily phase area as a function of time is also shown in Figure 5. The slope of this curve is similar for both Experiments A and B. Towards the end of the experiments, the great island appearing in the Experiment A is almost 30 cm^2 larger than the island in the Experiment B. This is the main reason, because the final trapped oil percent was different; 22.3% for Experiment A and 13.3% for Experiment B.

Experiments with G = 0.075 (C and D). In Experiments C and D (Figure 2) the oil-water interface did not reach the outlet at the final stage. This particular behavior may be related to smaller capillary forces and higher static pressure head due to a larger gap than that in previous experiments; therefore, the water-oil interface did not reach the cell outlet in spite of the enough elapsed time for each experiment.

The behavior of the total oily phase area is shown in Figure 5 for Experiments C and D. In both experiments, islands were hardly formed. Although the experiments had certain similarity in the first 10 min, their subsequent behavior was different. In Experiment C the displacement after 10 min became slower than in D, as may be appreciated in the slope of the curve. A notorious difference in the trapped oil percent towards the end of the experiments might be appreciated: 92.2% for the Experiment C and 72.8% for the Experiment D.

Sweep Efficiency Observed in All of the Experiments. Higher oil recovery percentages were obtained in the Experiments A and B, for G = 0.015 (77.7% and 86.7%, respectively), followed by Experiments E and F with G = 0.005 (70.4% and 64.5%, respectively). Although the displacement for G = 0.005 was faster than the displacement for G = 0.015, more scattered oil drops were left trapped behind and a counter-current oil flow took place, expelling the oil trapped close to the inlet. This was observed to happen after the outlet was water-flooded (Figure 4, last slide of each experiment). A similar behavior is observed in porous models by Chatzis et al. (1983), as an increasing trapping with a decreasing porosity. On the other hand, a uniform interface sweep was found for G = 0.075, Experiments C and D. However, the oil recovery was reduced to less than a third of the total oil volume (7.8% and 27.2%, respectively).

Interfacial dynamic analysis

The water-oil interface behavior is analyzed in this section in relationship to the oil expulsion rate. This is according to the continuous and insular region definitions. The water-oil interface at the continuous region is a curved line closely coincident with the water-oil-glass contact lines. The line tension at the contact lines is responsible for the spontaneous displacement. The insular region perimeter is not associated with the fluid dynamics, except when the insular phase is in transient, migrant, splitting, or coalescing stages. It was frequently observed that the water-oil interfacial length was a growing function of time, whose initial value was similar to the inlet edge length (~ 19 cm) and whose evolution might present several peaks.

The continuous region area and the water-oil interfacial length as functions of time, for Experiments A, C and E, are shown in Figure 6. The growth of the water-oil interfacial length was observed and was accompanied by a decline in the continuous region area. At the beginning, when the interface had been scarcely distorted, the continuous region area was only slightly reduced. However, when the water-oil interfacial length was growing notoriously, a significant decrease of the continuous region area was observed. This is an indication of the oil expulsion rate dependence on the growth rate of the water-oil interfacial length. The peaks in the water-oil interface curve were due to the fragmentation of big islands from the continuous region, causing a sudden decrease in the water-oil interfacial length of the continuous region.

During the fluid displacement, more interfacial length was always generated and, although the insular region did not contribute to the motion, it provided an interfacial perimeter that increased as time elapsed. In some cases, the water-oil interfacial length decreased even though the insular region had been growing, due to the fact that the insular region

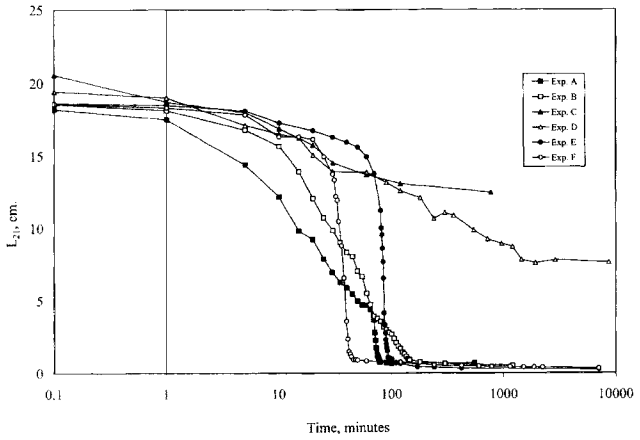

Figure 7. L_{21} = oil total area/water-oil total interfacial length ratio vs. time.

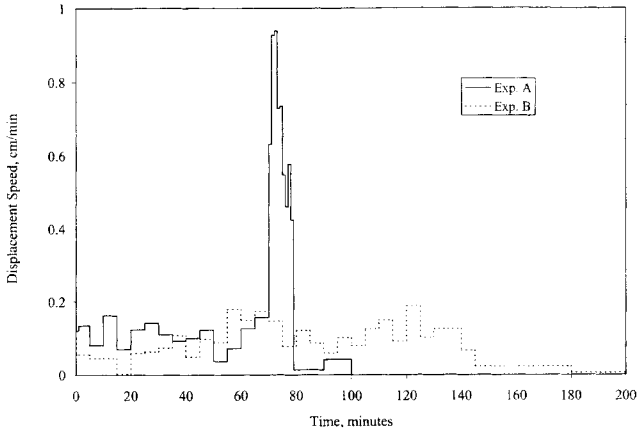

Figure 9. Displacement speeds for Experiments A and B.

modified its interfacial perimeter by migration, splitting, coalescence or by oil expulsion toward the outlet or inlet to the cell.

Notorious differences between experiments with different gap are apparent from an inspection of the sequences shown in Figures 2 to 4. From these observations, it could be proposed that the behavior of the oil displacement by water resulted in a different pattern for each gap. One of the relevant characteristics of such patterns is the island formation, which at the same time, produces a significant amount of interfacial perimeter. Another relevant observation is the fingering of interfacial length generation. These facts suggest that a relevant variable for the displacement pattern characterization for the several gaps should be a characteristic interfacial length L_{21}, defined by

$$L_{21} = (\text{Oil total area})/(\text{Water-oil total interfacial length})$$

The behavior of this variable as a function of time is shown on a time logarithmic scale, in order to better visualize the initial changes, in Figure 7. The experiments were found to have similar behavior for each gap. In order to quantify this similarity the slope of the largest decreasing region was obtained. These slopes are -157.26 and -85.01 for experiments E and F, respectively; -9.41 and -13.37 for experiments A and B, respectively; and -3.01 and -3.57 for experiments C and D, respectively.

Taking the average slope for each gap the mean values were: -121.14 for G = 0.005, -11.39 for G = 0.015, and -3.29 for G = 0.075. Pronounced slopes can be associated to small gaps, while small slopes can be associated to large gaps and intermediate slopes correspond to intermediate gaps. Despite the initial and final effects, shown in Figure 7, it is possible to identify a characteristic pattern for each gap. In these patterns, the water displacement rate depends on a different interfacial length rate generation for each gap.

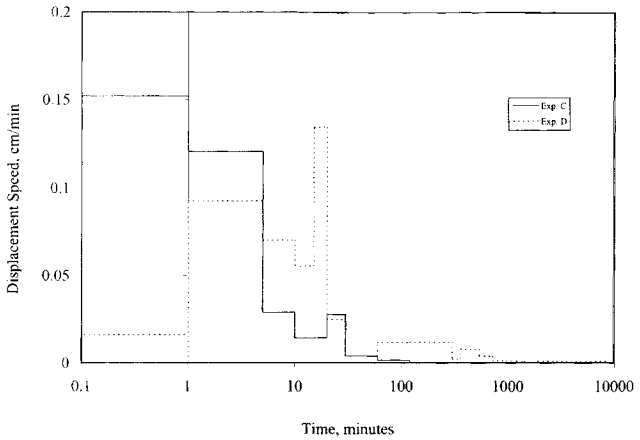

Figure 8. Displacement speeds for Experiments C and D.

Analysis of the fluid displacement

Finally, the spontaneous flow behavior was studied in order to find displacement patterns according to the cell gap. The average displacement speed for water in a given time interval was used as the significant variable, defined according to the equation

$$V_i = (A_{i+1} - A_i)/(t_{i+1} - t_i)W \qquad (1)$$

where V_i is the forward difference average displacement speed at time t_i, A_i is the total water area at time t_i, A_{i+1} the total water area at time t_{i+1}, and W is the cell width. In Figures 8, 9 and 10, the behavior of V_i is shown.

According to the visual inspection of both the displacement process (Figures 2 to 4) and the speed behavior (Figures 8, 9 and 10), two or three evolution stages might be identified. Experiments with fingering (A, B, E, and F in Figures 9 and 10) presented three stages: an *initial stage* occurring at the beginning of the experiments, when a slightly uniform advance front is developed, followed by a *development stage*, which began with a continuous increasing speed and the incipient finger formation which can be distinguished as small growing up bumps that developed a fast accelerating-decelerating process, and a *third stage* with important outlet

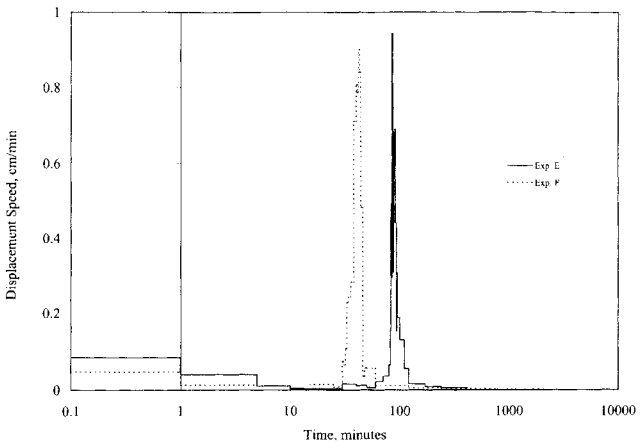

Figure 10. Displacement speeds for Experiments E and F.

effects was also found, but its analysis was left for a further study. Two stages were identified for experiments with G = 0.075. A continuous speed decay down to a static condition was the pattern followed by experiments C and D. An initial and a final asymptotes were found and their intersection was taken as a point to define two asymptotic stages. An *initial stage* before the intersection point and a final stage after it.

Experiments with G = 0.075. The displacement speed for Experiments C and D is also shown in Figure 8. Its decrease until the displacement stops is apparent. Two sequential characteristic values for speed were identified. A notorious displacement speed decrease was observed the first 20 min for Experiment C, while, after an initial low speed that increased at 1 min, a further decrease was observed the next 14 min for Experiment D. This was followed by a smaller speed behavior, after a sudden acceleration-deceleration event that might be understood as an incident development stage which could not be developed. If this event is considered together with the final stage, the times for this stage can be seen in Table 2.

Experiments with G = 0.015. The speed behavior of Experiment A was somewhat different from Experiment B, in spite of their similar configurations. A slightly uniform front with short fingers was formed during the first 50 min for both experiments, with small values of the displacement speed, followed by the development of a front with one finger at first. This finger developed earlier in Experiment B, followed by another later finger on the opposite side of the cell. In Experiment A, the first finger did not have a sensitive development, but this was not until another finger was formed on the opposite side and then both fingers evolved at the same time. This fact caused a difference in the displacement speed, as can be appreciated in Figure 9, where the simultaneous fingering development in Experiment A appears as a fast increase in displacement speed at 70 min, preceded by a continuous increase during 15 min, while, in Experiment B, a slower first increase had a maximum at 55 min, preceded by an increase from 20 min, which was followed by a decay and a further second increase at 95 min. The development stage beginning and duration are reported in Table 2. The double values of duration in the development stage for Experiment B take account of the two consecutive fingers. The decelerating stages might be associated with the proximity of the finger nose to the outlet. When this happened, the deceleration occurred together with a bump appearance, growing up towards the cell center. Finally, the fingers approached each other and coalesced with a small displacement speed, giving rise to a large island at the cell center, towards the end of both experiments. The end of the development stage was coincident with that approaching between both fingers towards the end of the decelerating speed event, as can be observed in Table 2, by the summation of the time intervals.

Experiments with G = 0.005. A very poor, but slightly uniform, advance was observed at the beginning of both experiments with a constant displacement speed (Figure 10). After an incipient fingering formation, an explosive breakthrough was observed for Experiment E and Experiment F. The times at the breakthrough correspond to the end of the initial stage and are reported in Table 2. These times marked the beginning of the development stage. Fingering was found responsible for the sudden increase in the displacement speed and a deceleration time interval occurred later, when the finger nose reached the outlet and spread onto the outlet zone. The end of the development stage is marked by the end of the decelerating speed, whose duration is reported in Table 2.

Averaged Parameter Comparison. Based on the above analysis, an average characteristic displacement speed for each stage was found by averaging the values of V_i given by Eq. 1 and a characteristic advancement length L_A was estimated from Eq. 2 for each stage, where the subscripts *initial*

Table 2. Displacement Speed, Advancement Length and Elapsed Time for Initial and Development (or Final) Stages

Glass Sheets Gap cm	Experiment	Av. Speed, cm/min		Av. Length, cm		Time interval, min	
		Init. Stage (V_I)	Dev. Stage (V_D)	Init. Stage (L_{AI})	Dev. Stage (L_{AD})	Init. Stage (t_I)	Dev. Stage (t_D)
0.005	E	0.016	0.23	1.290	9.167	80	40
	F	0.011	0.41	0.340	7.314	30	18
0.015	A	0.11	0.32	5.851	7.737	55	24
	B	0.037	0.10 0.12 Final Stage (V_F)	0.742	7.654 5.763 Final Stage (L_{AF})	20	75 50 Final Stage (t_F)
0.075	C	0.084	0.0056	1.675	0.620	20	110
	D	0.067	0.0025	1.012	3.529	15	1425

Table 3. Displacement Speed and Advancement Length Ratios*

Gap	0.005 cm		0.015 cm			0.075 cm	
Experiment	E	F	A	B		C	D
Ratio V_I/V_D	0.070	0.027	0.34	0.33	V_I/V_F	14	27
Ratio L_{AD}/G	2000	1000	520	890	L_{AF}/G	13	47
Initial Stage Average Displacement Speed, $\langle V_I \rangle$, cm/min	0.014		0.08			0.076	
Development Stage Displacement Average Speed, $\langle V_D \rangle$, cm/min	0.32		0.22		Final Stage	0.0041	
Initial Stage Ca	3.2 E-7		18 E-7			18.E-7	
Development Stage Ca	78.E-7		52. E-7		Final Stage	1.0 E-7	
Initial Stage IPD	1654.4		370.5			1.4	
Development Stage IPD	69.8		126.6		Final Stage	26.0	

*Also averaged displacement speed, Ca and IPD for initial and development (or final) stages.

and *final* refer to each particular stage. The results are shown in Table 2

$$L_A = (A_{\text{final}} - A_{\text{initial}})/W \tag{2}$$

The following observations should be emphasized from the results in Table 2. The average displacement speed at the initial stage has always lower values than those for the development stage for Experiments A, B, E and F (experiments with fingering). In Experiments C and D the opposite behavior is observed; the initial stages present higher values as compared with the corresponding final stages. The double values for the development stage of Experiment B in Table 2 are those that correspond to the first and the second finger appearance.

Two dimensionless ratios were estimated from Table 2 and shown in Table 3. The following facts could be established: for G = 0.005 the initial speed was in average 5% of the development speed, while for experiments at G = 0.015, this ratio was around 34%. For experiments at G = 0.075, the initial speed to final speed ratio was around 2,000%. This observation is an indication of a significant difference in the flow pattern for the initial stage to the development stage (or the final stage) depending on the cell gap.

The ratios for the estimated lengths at the development and final stages, divided by the cell gap, are also shown in Table 3. The development and final length $L_{AD,F}/G$ seem to have a decreasing dependence on the glass sheets gap, since its average for same gap experiments is 1,500 for G = 0.005, 700 for G = 0.015, and 30 for G = 0.075. However, this is not conclusive since experiments with larger cells are in order to reduce outlet effects.

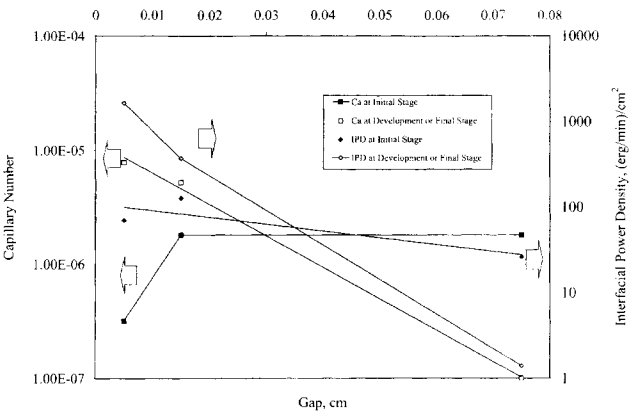

Figure 11. Capillary number (Ca) and interfacial power density (IPD) for initial and development or final (G = 0.075) stages.

For experiments with the same gap, the average characteristic displacement speed for each stage was averaged for both experiments with the same gap, and the relationship between viscous and capillary forces was evaluated through the capillary number ($Ca = \langle V \rangle \mu/\sigma$) with the viscosity and interfacial tension, taken as constants, the results are also shown in Table 3.

It is interesting to note that while the capillary number at the initial stage increases with the glass sheet gap, the capillary number at the development stage decreases as the gap increases. There should be a crossover of both capillary number values between G = 0.015 and G = 0.075.

Since fingering is associated with high capillary numbers (Coniglio, 1990), as may be observed in the development stage for G = 0.005 and G = 0.015, it may be speculated that fingering occurs for smaller gaps than the one which corresponds to the crossover of the initial and development capillary numbers. This crossover may occur somewhere around G = 0.030 for a capillary number of approximately 1.8 E-6, as is shown in Figure 11. Experimental research on this topic is an objective for further work.

Since capillary force is the driving force for spontaneous imbibition, *the interfacial power density* (IPD) defined as an amount in the order of $\langle V \rangle \sigma/G$, is a relevant quantity for this process. In Figure 11 the initial and development IPD's are plotted as functions of the gap. It is apparent there that the initial IPD has a crossover with the development IPD at G = 0.035. The development IPD is a decreasing function of the gap. Therefore, it is possible to strengthen the hypothesis previously established that a fast fingering advance is possible for gaps smaller than this value, since the Development IPD is greater than the initial one. Otherwise, a decay of spontaneous imbibition should be observed, for gaps greater than G = 0.035, since the development IPD is smaller than the initial one. It is also remarkable that the initial IPD is only slightly dependent on gap, with an average value close to 74 (erg/min)/cm^2. This fact is a help to roughly estimate the initial average speed, given a glass sheet gap.

The experimental findings of this study allow us to set that the maximum recovery in Hele-Shaw cells is not only due to the separation, but also to the dynamic behavior of the island formation and to the fingers evolution. Therefore, it should not be considered that the greater the capillary force, the better the oil recovery, since the formation of many islands could prevent the efficiency recovery to be as much as it might be expected. It also should be noted that the fast finger advancing could block the outlet early, generating a backwards oil flow and oil entrapment that should drop down the oil recovery efficiency. Moreover, for greater sheet separations, the capillary force is very weak and forced imbibition should be the only way to drive water into the medium after a short spontaneous imbibition process took place, leaving the spontaneous imbibition as the main mechanism at the porous medium only. These conclusions might be useful for the secondary recovery processes in fractured water-wet reservoirs. However, we acknowledge that many specific studies are yet needed. It should be pointed out that although the reported results are not scalable to naturally fractured reservoir conditions, it is yet possible to determine the governing mechanisms and behavior in spontaneous imbibition processes. These mechanisms should be considered in the matrix-fracture interaction models in order to obtain better predictions and make contributions to the optimization of secondary oil recovery processes.

Conclusions

Repeatability

The spontaneous displacement process of oil (Soltrol 170) by twice-distilled water can approximately be repeated. A scrupulous cleaning procedure was able to restore the glass sheets original wettability. The displacement pattern and rate for every experiment and its repetition has a similar behavior that depended on the cell gap. The optimum oil recovery was achieved for a $G = 0.015$.

Waviness

Natural glass surface waviness is too small, as compared to the cell gap, in order to make significant contributions to the spontaneous imbibition flow patterns. A significant change in the displacement pattern can be generated only by a significant change in the glass sheet gap.

Water-oil interface length

For each gap, a defined behavior of the (oil total area)/(water-oil total interfacial length) ratio was found. For a $G = 0.005$, the slope was -121.14 cm. For a $G = 0.015$, the slope was -11.39 cm, and for a $G = 0.075$ the slope was -3.29 cm. The interfacial length growth is the mechanism for spontaneous displacement of oil by water, because it occurred with a continuous interfacial length generation before outlet effects could be detected. This is an indication of the oil expulsion rate dependence on the growth rate of water-oil interfacial length. Neglecting the outlet effects, it seems that there is no way for the interface to advance without increasing its magnitude.

Types of flow

The spontaneous displacement speed showed three consecutive stages for $G = 0.015$ and for $G = 0.005$: a first one was named the initial stage with a slightly uniform front interface displacement, a second one was named the development stage with fingering displacement, and a third one was named the final stage with outlet interaction. Two stages were observed for the displacement speed for $G = 0.075$: a first one or the initial stage, faster than a second one or the final stage. The initial stage speed to the development stage speed ratio was evaluated for each gap: For $G = 0.005$, the ratio was approximately 5%; for $G = 0.015$, it was around 34% and, for $G = 0.075$, it was around 2,000%.

Capillary number

The average displacement speed at the development stage for each gap was 0.22 cm/min for $G = 0.005$, 0.32 cm/min for $G = 0.015$, and 0.0041 cm/min for $G = 0.075$. A fingering displacement in the development stage appeared for $G = 0.015$ and smaller. For $G = 0.075$, the displacement is slightly uniform and the speed decreases until static equilibrium is reached. The capillary number at the initial stage increases with the glass sheet gap for smaller gap values and stays constant for $G \geq 0.015$. At the development and final stages, the capillary number decreases as the gap increases. There should be a crossover around $G = 0.030$ for both capillary number values.

Interfacial power density

The initial interfacial power density is only slightly dependent on gap, with an average value close to 74 (erg/min)/cm^2, while the development interfacial power density is a decreasing function of the gap. A fast fingering advance is possible for gaps smaller than 0.035 cm, otherwise a decay of spontaneous imbibition should be observed after the Initial stage.

Acknowledgments

This research was supported by Instituto Mexicano del Petróleo through the research projects FIES 95-92-I and 97-07-1. The authors are also indebted to the Thermodynamics Laboratory group at the Universidad Autónoma Metropolitana, Unidad Iztapalapa. Special acknowledgments are due to Dr. Francisco Guzmán López-Figueroa who allowed us the use of laboratory facilities for this research project and many fruitful discussions on the experimental setup. Also we greatly benefit from the review and discussions of Dr. Gretchen Lapidus. The authors also benefited from a Negromex financial aid at the former stage of the project.

Literature Cited

Akin, S., J. M. Schembre, S. K. Bhat, and A. R. Kovscek, "Spontaneous Imbibition Characteristics of Diatomite," *J. of Pet. Sci. and Eng.*, **25**, 149 (March 2000).

Aronofsky, J. S., L. Massé, and S. G. Natanson, "A Model for the Mechanism of Oil Recovery from the Porous Matrix Due to Water Invasion in Fractured Reservoirs," *Pet. Trans. AIME*, **213**, 17 (1958).

Bech, N., O. K. Jensen, and B. Nielsen, "Modeling of Gravity-Imbibition and Gravity-Drainage Processes: Analytic and Numerical Solutions," *SPERE*, 129 (Feb., 1991).

Beckner, B. L., K. Ishimoto, S. Yamaguchi, A. Firoozabadi, and K. Azizet, "Imbibition-Dominated Matrix-Fracture Fluid Transfer in Dual Porosity Simulators," Technical Conf. and Exhibition of SPE Proc., Dallas, p. 509 (Sept. 27–30, 1987).

Bobek, J. E., C. C. Mattax, and M. O. Denekas, "Reservoir Rock Wettability—Its Significance and Evaluation," *Pet. Trans. AIME*, **213**, 155 (1958).

Bourbiaux, B. J., and F. J. Kalaydjian, "Experimental Study of Cocurrent and Countercurrent Flows in Natural Porous Media," *SPE Reservoir Eng.*, 361 (Aug., 1990).

Brownscombe, E. R., and A. B. Dyes, "Water-Imbibition Displacement...Can it Release Reluctant Spraberry Oil," *Oil and Gas J.*, 264 (Nov. 17, 1952).

Cuiec, L. E., B. Bourbiaux, and F. Kalaydjian,"Imbibition in Low-Permeability Porous Media: Understanding and Improvement of Oil Recovery," *Symp. on EOR Proc.*, Tulsa, OK, SPE/DOE No. 20259, 833 (Apr. 22–25, 1990).

Chatzis, I., N. Morrow, and H. T. Lim, "Magnitude and Detailed Structure of Residual Oil Saturation," *SPEI*, 311 (Apr., 1983).

Chatis, I., and F. A. L. Dullien, "Dynamic Immiscible Displacement Mechanism in Pore Doublets: Theory versus Experiment," *J. of Colloid and Interface Sci.*, **91**, 199 (1983).

de Swaan, A., "Theory of Water-Flooding in Fractured Reservoirs," *Soc. of Pet. Eng. Soc. J.*, **265**, 117 (Apr., 1978).

de Swaan, A., and M. Ramírez, "Functions of Flow from Porous-Rock Blocks," Unsolicited paper, SPE No. 20173 (1990).

de Swaan, A., "Simple Models of Water Imbibition and Gravitational Drainage of Oil in Rock Blocks," SPE *Int. Petroleum Conf. and Exhibition of México Proc.*, Villahermosa, México, SPE No. 39829 (Mar. 3–5, 1998).

Dussan, E. B., E. Ramé, and S. Garoff, "On-Identifying the Appropriate Boundary Conditions at a Moving Contact Line: an Experimental Investigation," *JFM*, **230**, 97 (1991).

Hayashi, J. A., "Procesos de Imbibición Espontánea en Celdas Hele-Shaw," PhD Diss., Universidad Autónoma Metropolitana-Iztapalapa (2001).

Hayashi, J. A., and C. Pérez-Rosales, "Visual Investigation of Imbibition Processes," LAPEC SPE Proc., Caracas, Venezuela, SPE No. 23745, 353 (Apr. 5–7, 1992).

Hayashi, J. A., and A. Soria, "Estudio Experimental del Flujo a Cocorriente y a Contracorriente en Procesos de Imbibición Espontánea, Utilizando Celdas Porosas Bidimensionales," *Avances en Ingeniería Química*, **5**, 272 (1995).

Jacquin, Ch., and B. Legait, "Influence of Capillarity and Viscosity During Spontaneous Imbibition in Porous Media and in Capillaries," *PCH PhysicoChemical Hydrodyn.*, **5**, 307 (1984).

Kalaydjian, F., and B. Legait, "Effects de la Géométrie des Pores et de la Mouillabilité sur le Déplacement Diphasique à Contrecourant en Capillaire et en Milleu Poreux," *Revue Phys. Appl.*, **23**, 1071 (1988).

Kazemi, H., L. S. Merril, K. L. Porterfield, and P. R. Zeman, "Numerical Simulation of Water-Oil Flow in Natural Fractured Reservoirs," *SPE J.*, 317 (Dec., 1976).

Kleppe, J., and R. A. Morse, "Oil Production from Fractured Reservoirs by Water Displacements," *49th Ann. Fall Meeting SPE-AIME Proc.*, Houston, TX, SPE No. 5084 (Oct. 6–9, 1974).

Lefebvre du Prey, "Gravity and Capillary Effects on Imbibition Porous Media," *SPE J.*, SPE No. 6192, 195 (June, 1978).

Mattax, C. C., and J. R. Kyte, "Imbibition Oil Recovery from Fractured, Water-Drive Reservoir," *SPE J.*, 177 (June, 1962).

Ramírez, M. A., "Estudio Experimental de la Imbibición Espontánea en Medios Capilares," M.Sc. Diss., ESIQIE, IPN (Dec., 1998).

Reis, J. C., and M. Cil, "Analytical Models for Capillary Imbibition: One Dimensional Matrix Blocks," *IN SITU*, **23**, 265 (1999).

Reis, J. C., and S. A. Haq, "Water Advance in a Single Fracture in the Presence of Capillary Imbibition into Adjacent Matrix Blocks," *IN SITU*, **23**, 271 (1999).

Rodríguez, F., "Modelo Analítico del Desplazamiento Lineal de Aceite por Inyección de Agua en Yacimientos Naturalmente Fracturados," *Ingeniería Petrolera*, **20** (June, 1988).

Rossen, R. H., and E. I. C. Shen, "Simulation of Gas/Oil Drainage and Water/Oil Imbibition in Naturally Fractured Reservoirs," *SPE Reservoir Eng.*, 464 (Nov., 1989).

Saidi, A. M., "Simulation of Naturally Fractured Reservoirs," SPE 12270, *Proc. Reservoir Simulation Symp. Proc.*, San Francisco, CA, 361 (Nov. 15–18, 1983).

Spildo, K., and J. S. Buckley, "Uniform and Mixed Wetting in Square Capillaries," *J. of Petroleum Sci. and Eng.*, **24**, 145 (1999).

Terez, I. A., and A. Firoozabadi, "Water Injection in Water-Wet Fractured Porous Media: Experiments and a New Model with Modified Buckley-Leverett Theory," *SPE J.*, **4**, 134 (June, 1999).

Zhang, X., N. R. Morrow, and S. Ma, "Experimental Verification of a Modified Scaling Group for Spontaneous Imbibition," *SPERE*, 280 (Nov., 1996).

Manuscript received Oct. 12, 1999, and revision received Oct. 17, 2000.